HHS Public Access

Author manuscript

Clin Genet. Author manuscript; available in PMC 2018 January 12.

Published in final edited form as:

Clin Genet. 2016 December ; 90(6): 509–517. doi:10.1111/cge.12785.

Autosomal Recessive IFT57 hypomorphic mutation cause ciliary transport defect in unclassified oral-facial-digital syndrome with short stature and brachymesophalangia

Julien Thevenon[1,2,3,*], **Laurence Duplomb**[1,2,*], **Shubha Phadke**[4], **Thibaut Eguether**[5], **Aline Saunier**[6], **Magali Avila**[1,2], **Virginie Carmignac**[1,2], **Ange-Line Bruel**[1,2], **Judith St-Onge**[1,2,7], **Yannis Duffourd**[1,2], **Gregory J. Pazour**[5], **Brunella Franco**[8,9], **Tania Attie-Bitach**[10], **Alice Masurel-Paulet**[1,3], **Jean-Baptiste Rivière**[1,2,7], **Valérie Cormier-Daire**[10], **Christophe Philippe**[6], **Laurence Faivre**[1,2,3], and **Christel Thauvin-Robinet**[1,2,3]

[1]FHU-TRANSLAD, Université de Bourgogne/CHU Dijon; France

[2]Equipe EA4271 GAD, Université de Bourgogne, Dijon, France

[3]Centre de Référence maladies rares « Anomalies du Développement et syndrome malformatifs » de l'Est et Centre de Génétique, Hôpital d'Enfants, CHU, Dijon, France

[4]Department of Medical Genetics, Sanjay Gandhi Post Graduate Institute of Medical Sciences, Lucknow, Uttar Pradesh, India

[5]Program in Molecular Medicine, University of Massachusetts Medical School, Worcester, Massachusetts, USA

[6]Laboratoire de Génétique Médicale, CHU - Hopitaux de Brabois, 54511 Vandoeuvre les Nancy cedex, France

[7]Laboratoire de Génétique Moléculaire, PTB, CHU Dijon, Dijon, France

[8]Telethon Institute of Genetics and Medicine-TIGEM, Naples, Italy

[9]Department of Medical Translational Sciences, Division of Pediatrics, Federico II University of Naples, Italy

[10]Service de Génétique, Hôpital Necker-Enfants Malades, APHP, Institut Imagine, INSERM UMR1163, University Sorbonne-Paris-Cité, Paris, France

Abstract

Corresponding author: Julien Thevenon, MD-PhD, Centre de Génétique, Hôpital d'Enfants, 10 Bd du Maréchal de Lattre de Tassigny, 21034 Dijon cedex, France, tel: 33 3 80 29 53 13, fax: 33 3 80 29 32 66, julien.thevenon@chu-dijon.fr.

Conflict of Interest Statement

There are no conflicts of interest to declare.

Web Resources

Homozygosity mapping: www.homozygositymapper.org.
NHLBI Exome Sequencing Project Exome Variant Server, http://evs.gs.washington.edu/EVS/
dbSNP, http://www.ncbi.nlm.nih.gov/projects/SNP/
Picard, www.picard.sourceforge.net
University of Burgundy Centre de Calcul, https://haydn2005.u-bourgogne.fr/dsi-ccub/Seattle Seq Annotation tool: snp.gs.washington.edu/SeattleSeqAnnotation137/

The 13 subtypes of oral-facial-digital syndrome (OFDS) belong to the heterogeneous group of ciliopathies. Disease-causing genes encode for centrosomal proteins, components of the transition zone or proteins implicated in ciliary signaling. A unique consanguineous family presenting with an unclassified OFDS with skeletal dysplasia and brachymesophalangia was explored. Homozygosity mapping and exome sequencing led to the identification of a homozygous mutation in IFT57, which encodes a protein implicated in ciliary transport. The mutation caused splicing anomalies with reduced expression of the wild type transcript and protein. Both anterograde ciliary transport and sonic hedgehog signaling were significantly decreased in subjects' fibroblasts compared to controls. Sanger sequencing of IFT57 in 13 OFDS subjects and 12 subjects with Ellis-Van Creveld syndrome was negative. This report identifies the implication of IFT57 in human pathology and highlights the first description of a ciliary transport defect in OFDS, extending the genetic heterogeneity of this subgroup of ciliopathies.

INTRODUCTION

Oral-facial-digital syndromes (OFDS) are characterized by malformations of the face, oral cavity and extremities [1]. Clinically, OFDS may be diagnosed by the presence of: i) oral anomalies such as tongue hamartomas, oral frenulae, cleft palate, abnormal teething; ii) facial dysmorphism such as hypertelorism, lateral or medial cleft lip and iii) digital anomalies such as pre-, meso- or post-axial polydactyly, abnormal Y-shaped metacarpes, or syndactylies. Besides these common features, each sub-type of OFDS bears clinical hallmarks, namely polycystic kidney disease (OFDI), hallux valgus and normal intelligence (OFDII), tibia anomalies (OFDIV), cerebellar hypoplasia with the molar tooth sign (OFDVI) and coloboma (OFDIX) [2]. Among the 13 clinical subtypes, inheritance is autosomal recessive in most subtypes except OFDI. While most OFDS are ciliopathies caused by mutated centrosomal proteins (OFD1, SCLT1 and TBC1D32/C6orf170) or components of the transition zone (TMEM216 and TCNT3) [3–6]. Mutations in some OFD genes have also been reported in overlapping ciliopathies such as Joubert Syndrome and Related Disorders (JSRD)/Meckel syndrome (OFD1, C5orf42, TMEM216 and TCNT3) [6–8].

Clinical entities secondary to mutations in genes encoding for proteins implicated in ciliary transport are represented by the short-rib polydactyly syndromes (SRPS), which includes at least 6 distinct entities [9]. Among these, Ellis-Van Creveld syndrome (EVCS) is distinct from the others by the presence of post-axial polydactyly, congenital cardiac defects, mesomelic limb shortening, short ribs, dysplastic nails and teeth, and labio-gingival adhesion [9]. In 1999, Phadke et al. reported a unique consanguineous family with 3 affected siblings presenting with clinical features overlapping between OFDS and EVCS [10]. This family was reassessed and the causal gene mutation of this untyped OFD syndrome was identified by homozygosity mapping and exome analysis.

METHODS

Homozygosity mapping and exome sequencing

Two affected siblings (Subject II-1 and II-2, Figure 1A) were genotyped with an Affymetrix 250K NspI array (Affymetrix, Santa Clara, California, USA). Array experiments and

analysis were conducted according to protocols from the manufacturer and with Homozygosity Mapper, respectively (See Web Resources). Homozygous stretches of more than 1 megabase with quality over 250 were selected (arbitrary unit from homozygosity mapper software). Exome sequencing was performed on Subject II-1 (Figure 1A) according to standard procedures using the Nimblegen SeqCap EZ Exome v2.0 kit, from 8 μg of DNA sample from affected individuals and both parents. The resulting exome-capture libraries underwent 2×100-bp paired-end sequencing on an Illumina HiSeq 2000. Reads were aligned to the human reference genome (GRCh37/hg19) with the Burrows-Wheeler Aligner (BWA, v0.5.6) [11] and potential duplicate paired-end reads were removed using the picardtools v1.22 (see Web resources). The Genome Analysis Toolkit (GATK) 1.0.57 was used for base quality score recalibration and indel realignment [12], as well as for single-nucleotide variant and indel discovery and genotyping using standard hard filtering parameters. Variants with quality scores of <30, sequencing depth of <4, quality/depth ratio of <5.0, length of homopolymer run of >5.0 and strand bias of >−0.10 were flagged and excluded from subsequent analyses. Coverage was assessed with the GATK Depth of Coverage tool by ignoring reads with mapping quality of <20 and bases with base quality of <30. All variants identified in the affected individuals were annotated with SeattleSeq SNP annotation (see Web resources). Candidate variants were selected by fulfilling the following criteria: i) variants included in the previously identified homozygous intervals (defined with allele balance from 75% to 100% of the reads supporting the variant), ii) variants affecting in the coding sequence, iii) rare variants, absent from 50 local exomes of unaffected individuals and present at a frequency below 1% in dbSNP 138 and the NHLBI GO Exome Sequencing Project (See Web Resources).

Sanger sequencing in the replicative cohort

IFT57 primers were designed on the RefSeq NM_018010 (Table S1). PCR fragments were purified with the multiscreen Vacuum Manifold system (Millipore). Sequencing was performed with the ABI BigDye Terminator Cycle Sequencing kit (v.3.1) (Applied Biosystems) in ABI 3130 sequencer 7 (Applied Biosystems) according to the manufacturer's instructions. Sequence data were analyzed with SeqScape v.2.7 (Applied Biosystems).

Cell culture—Fibroblasts from healthy controls and the IFT57 mutated subject (Subject II-1, Figure 1A) were obtained after written consent for skin biopsy. Cells were cultured in DMEM supplemented with 10% fetal calf serum (FCS) and 1% penicillin/streptomycin (P/S) and were grown at 37°C in a 5% CO2 atmosphere. For cilium induction, cells were FCS-starved for 48 hours before subsequent analysis. For studies of the SHH pathway, cells were FCS-starved overnight, then stimulated with 1 μM Smoothened Agonist (SAG) (Merck Millipore, Darmstadt, Germany) for 30 hours [6].

ARN extraction and real-time RT-qPCR

Total RNA was extracted using TRI reagent® (Sigma, Saint Quentin Fallavier, France), according to the manufacturer's protocol. First strand cDNA was synthesized from 0.5μg total RNA using Maxima First Strand cDNA Synthesis Kit for RT-qPCR from Fermentas (Thermo Scientific). The real-time PCR contained, in a final volume of 20 μl, 2 ng reverse transcribed total RNA, SYBR green buffer (Bio-Rad, Marnes-la-Coquette, France), 300 nM

of the forward and reverse primers: and (Bio-Rad). PCRs were performed in triplicate in 96-well plates, using the CFX96 Real-Time PCR detection system (Bio-Rad). Human Glyceraldehyde 3-phosphate dehydrogenase (GAPDH) was used as an invariant control (Table S1).

Analysis of the IFT57 transcripts by RT-PCR and Sanger sequencing

Total RNAs from cultured fibroblast with the Kit QIAmp RNA Blood Mini kit (QIAGEN). RNA quality (RNA Integrity Number >9) was assessed with the Agilent 2100 Bioanalyzer. For inhibition of the nonsense mediated mRNA decay (NMD) pathway, fibroblast cells were grown for 12 h in DMEM GlutaMAX media (Gibco, Thermo Fisher Scientific) supplemented with 10% calf serum, in the presence of 200 μg/ml puromycin (SIGMA-Aldrich) and then harvested in lysis buffer prior to RNA extraction. Prior to RT-PCR, RNAs were treated with DNase I (Sigma) at room temperature for 15 min, DNase I was inactivated at 70°C for 10 min. RT-PCR was performed on total RNAs from fibroblasts with primers located in exon 2 (Forward 5′ TGATGACCCTAATGCAACAATATCT 3′) and exon 11 (Reverse 5′ GCCAATTCTAATGTCCATCTCTACA 3′) (NM_018010.3). with the QIAGEN OneStep kit. RT-PCR products were separated on 2% agarose gel and bidirectionally sequenced.

Ciliary transport

α-acetylated tubulin antibody was purchased from (Invitrogen, Thermo Scientific, France), IFT57 antibodies were generated in rabbit [13]. Cells were washed in PBS and fixed in 4% PFA for 20 min, incubated in NH4Cl 50 mM for 10 min, permeabilized in PBS/0.3% Triton for 7 min and blocked in PBS/0.1% Tween 20/3% BSA for 15 min. Incubations with primary antibodies were performed in PBS/0.1% Tween 20/3% BSA for 3 hours at room temperature. After 3 washes in PBS, incubations with appropriate secondary (Alexa-Fluor-488- and Alexa-Fluor-588-conjugated goat anti-mouse and goat anti-rabbit were performed for 1 hour at room temperature. After 3 washes, cells were mounted with FluorshieldTM with DAPI (Sigma).

RNA interference—Small interference RNAs (siRNA) against IFT57 and negative control siRNA (both siGENOME SMARTpool, sequences available on request) were purchased from ABgene Ltd (Thermo Scientific). Transfection of siRNA was obtained using Lipofectamine™ RNAiMAX reagent (Invitrogen) according to the manufacturer's protocol. Briefly, 0.1×106 fibroblasts from healthy controls were seeded in 2 ml of DMEM containing 1% P/S and 10% FCS. After 24 h, cells were FCS-starved and siRNA (100 pmol)/ lipofectamine™ RNAiMAX (5 μl) complexes (in 500 μl Opti-MEM® Medium) were added to the cells. The next day, SAG (1μM) was added for 30 hours. The efficiency of siRNA delivery against IFT57 was confirmed by RT-qPCR. IFT57 mRNA expression was decreased by 95% (n=3, data not shown).

SUBJECTS AND RESULTS

Subjects

Index family—The reported subjects born to healthy consanguineous parents (Figure 1A) were first published during childhood [10] and followed up for 15 years. Subject II-3 died at 17 years of age because of a complicated pulmonary infection.

Subject II-1 was interviewed at 25 years of age. Intelligence was normal. He had short stature with a final height of 155 cm (−3 SD), weight 45 kg (<−3 SD) and occipito-frontal circumference (OFC) 50 cm (mean). The clinical examination showed a square face with short forehead, upslanting palpebral fissures, high nasal bridge with pyriform nose above a short philtrum and a medial clefting of upper lip (Figure 1B). Oral anomalies included supernumerary frenulae and missing incisors. Digital anomalies included pronounced brachydactyly, upper-limb post-axial polydactyly. Lower limb extremities showed spacing between the first and second rays. There was no thoracic deformity. X-rays of the hands and feet showed severe mesophalangeal shortening. Pre-axial polydactyly was diagnosed, because of first metatarsal duplication. Bone studies showed bilateral short femoral necks with varus femurs, symmetric genu valgus and no vertebral anomalies. Heart, renal and abdominal ultrasound examinations were normal.

Subject II-2 was interviewed at 22 years of age. Intelligence was normal; she was married with no children. She had short stature with a final height of 122 cm (−5 SD), weight 37 kg (−2 SD) and a conserved OFC at 51 cm (mean). Clinical examination showed a square face with narrow forehead, enophtalmia with up-slanting palpebral fissures, broad nasal bridge. Facial features included bilateral hypopigmented pseudo-clefts associated with medial labial clefting and oral anomalies such as missing incisors and supernumerary frenulae (Figure 1C). Digital anomalies included marked brachydactyly, four-limb post-axial polydactyly, surgically removed during infancy. There was neither thoracic deformity, nor dolichostenomelia. Puberty was not delayed. Hand X-rays revealed mesophalangeal shortening and residual right hand post-axial polydactyly with fused proximal phalanges and bifid telephalanges. Foot X-rays revealed duplication of the first-ray metatarsus and absent intermediary phalanges, suggesting lower limb pre-axial polydactyly. Abnormal vertebral bodies with medial notches but no platyspondyly, bilateral cervical ribs without narrow thorax were also present. Long bones were gracile with shortened femoral neck. Brain MRI, abdominal and heart ultrasounds were normal.

Replication cohort

A replication cohort was collected: i) 13 subjects with OFDS selected from a franco-italian cohort. Inclusion criteria were the association of polydactyly and cleft lip/palate; ii) 12 subjects with EVCS negative for EVC1 and EVC2 screening; iii) Next-generation sequencing data of the exome or ciliome from more than 172 subjects with various ciliopathy phenotypes were consulted [6].

Genetic analysis and mutation characterization

Considering the parental consanguinity, homozygosity regions were screened using homozygosity mapping in subjects 1 and 2. This approach identified 11-megabase of shared runs of homozygosity spreading from chr3:104822019-111671862 and chr10:1372501-6029726 (Hg19) (Figure 2A). These homozygous intervals did not overlap with genes previously associated with a recessive ciliopathy.

Exome sequencing was performed on subject 2. Over 4.7 gigabases of mappable sequences were generated by exome sequencing, resulting in a depth of coverage of at least ten reads for 95% of RefSeq coding exons (Table S2). First, causative variants affecting genes previously implicated in OFDS and EVCS syndromes were searched. Then, exome data analysis focused on the 2 homozygosity regions identified by homozygosity mapping in Subjects 1 and 2. This strategy allowed the identification of 32 homozygous variants, and among these, 5 variants that affected the coding sequence (Table S2). Extended familial segregation with Sanger sequencing in Subject 3 excluded one of the 2 homozygous interval (i.e. a AKR1C3 missense variation (chr10: 5147835 C/A, p.Leu298Ileu) was found heterozygous in Subject 3). In the remaining interval, only 1 homozygous variation was represented at a frequency lower than 1/100 in ESP, namely an IFT57 synonymous variation (chr3:g.107910368C>T, c.777G>A, p.Lys259Lys, RefSeq accession number NM_018010.3). This variant was absent from the ExAC database (Exome Aggregation Consortium (ExAC), Cambridge, MA (URL: http://exac.broadinstitute.org) [February 2016 accessed]). Sanger sequencing confirmed the variation at a homozygous status in the 3 affected subjects. Considering the underrepresentation of Indian subjects in public databases of genomic variants, absence of the rare variants was verified in 50 healthy subjects from northern India. At least, IFT57 was considered for further analysis in this family (Figure 2C). The c.777G>A substitution affecting the last base of exon 6 induces a complex splicing pattern including the normal transcript (A) but also three pathological mRNAs resulting from exon(s) skipping (B, C, and D). The pathological transcripts are only detected after inhibition of the NMD pathway. As expecting with sequence variation affecting consensus splice sites, the c.777G>A mutation leads to exon 6 skipping. More unusually, this variation in exon 6 has a bearing on retention of exon 5 and 4 of IFT57 in fibroblasts. Skipping of exon 6 in IFT57 pre-mRNA might induces modifications of the RNA secondary structure with a cis-acting effect on inclusion of adjacent exons 4 and 5.

Sanger sequencing for the 11 coding exon and intron boundaries of IFT57 was performed on 25 OFDS and EVCS subjects. No causative mutation was identified. Exome or ciliome data from 172 subjects with various ciliopathy phenotypes did not identify any biallelic causative mutations.

Ciliary transport

Because the variant in IFT57 was predicted to alter splicing, we performed cDNA quantification. RNA isolated from the subject's fibroblasts had significantly less IFT57 mRNA than did that of controls (Figure 2D). This suggests that the mutation causes a partial splicing defect resulting in the degradation of the altered cDNA so that only a residual amount of the normal mRNA remains. We then determined whether the remaining wild type

IFT57 was sufficient for proper ciliary assembly. Fibroblasts from the subject and controls were stained for IFT57 and for cilia using an antibody against acetylated tubulin. Primary cilia number and length in fibroblasts from the subject with the IFT57 mutation were similar to those in controls (Figure 3A and B). However, significant differences were observed between the subject and controls for intraflagellar transport. In control fibroblasts, IFT57 staining was observed in the whole primary cilium, merging with the staining of α-acetylated tubulin (Figure 3A and B). In the subject's fibroblasts, staining of the ciliary tip with IFT57 was significantly decreased (90% versus 35%; $p<0.001$) while staining of the basal body of the primary cilium was significantly increased ($p<0.01$).

SHH pathway activation

Since ciliary assembly was not affected by the IFT57 mutation, we wondered whether ciliary transport defect altered sonic hedgehog (SHH) signaling. Stimulation of the SHH pathway by Smoothened Agonist (SAG) showed poor induction of Gli1 mRNA expression in fibroblasts from the IFT57-mutated subject compared with control fibroblasts (Figure 3C). This indicates that even though ciliary assembly is normal in these cells the reduction in IFT57 causes dysfunctional SHH signaling. To confirm this result, IFT57 mRNA expression was knocked down in control fibroblasts using siRNA technology, with an efficiency of 95% (data not shown). A 3.7 fold increase in GLI1 transcript expression was observed in siRNA control-transfected cells after 30 hours in the presence of SAG (Figure 3C) whereas no induction of Gli1 mRNA expression was observed in siRNA IFT57-transfected cells.

DISCUSSION

Here, we report on a unique consanguineous family with an unclassified type of OFDS with short stature and brachymesophalangia overlapping with EVCS, and caused by a homozygous hypomorphic mutation of IFT57, affecting splicing and altering protein function.

The family was first published as a new overlapping OFDS-EVCS phenotype based on the association of median clefting, oral frenulae, missing incisors, short stature with mesomelic shortening, and pre and post-axial polysyndactyly [10]. When reviewed, the clinical evaluation was in favor of an unclassified OFDS type associated with skeletal dysplasia rather than EVCS (Figure 1B–C). Indeed, the reported subjects did not present rib shortening or thorax narrowness/deformity, but displayed a short stature, brachymesophalangia and stocky femoral necks, which suggests a new OFDS subtype with skeletal dysplasia. OFDII could first be suspected because of hallux valgus and normal intelligence, but short stature was atypical. Thus, an unclassified type of OFDS was evoked, once more underlying the clinical and genetic heterogeneity of OFDS.

IFT57 was first reported as HIPPI (Huntingtin-Interacting-protein Hip1), a gene coding for a caspase activator in adult neurons, implicated in neuronal death in Huntington disease [14]. However, further analysis indicated that IFT57 is a subunit of intraflagellar transport complex B [15]. IFT complex B is composed of 16 proteins [16], and in mice, null mutations in components of this complex typically alter ciliary assembly, provoke ciliary transport defect, inappropriate Sonic Hedgehog (SHH) signaling and cause lethality at mid

gestation [17]. Consistently, null mutations in mouse Ift57 blocked ciliary assembly in the node. The affected embryos died during embryogenesis and showed ciliopathy features such as upper and lower limb polydactyly, failed fusion and reduced length of the maxillary processes, neural tube defects, exencephaly and left-right axis pattern defects [18]. Similarly, zebrafish mutants for IFT57 displayed anomalies typical of ciliopathies [19, 20].

In human pathology, disease-causing mutations in genes implicated in ciliary transport are mainly identified in the SRPS group of ciliopathies [9]. Most of the mutated genes are in the motor for retrograde transport and in IFT complex A. Complex B is underrepresented with few cases reported [21–23]. Among the 60+ cases reported with mutations in genes coding for ciliary transporters, bi-allelic truncating mutations were never observed [21, 24–29] suggesting that null alleles in IFT genes would cause a severe phenotype not compatible with early development. This observation supports the hypothesis of a mild clinical presentation caused by the splice-site mutation in our subject that reduced but did not completely block the synthesis of IFT57 message. Among the whole-exome sequencing data of 62 000 individuals, no homozygous loss-of-function mutations are reported, suggesting that it may lead to a lethal phenotype. Here, the reduced level of message and protein is still able to support ciliary assembly, but the cilia are defective in hedgehog signaling. It is likely that defective hedgehog signaling underlies many of the phenotypes in our subject, as hedgehog signaling is critical for bone, digit and cranial facial development [30]. There is literature evidence for the role of IFT57 in retinal physiology, suggesting that there might be an ophthalmological involvement such as a retinopathy in the patients. However, these three individuals did not have visual complaints and there was no exclusion of ophthalmological involvement such as a retinopathy [31].

In conclusion, we report on a unique consanguineous family with 3 affected siblings with an unclassified OFDS subtype with short stature and brachymesophalangia, harboring a homozygous *IFT57* hypomorphic splice mutation altering ciliary transport defect and SHH signaling pathway.

Supplementary Material

Refer to Web version on PubMed Central for supplementary material.

Acknowledgments

We thank the family for their participation. This work was supported by grants from GIS-Institut des Maladies Rares for high-throughput-sequencing approach, the French Ministry of Health (PHRC national 2010 and 2012), Dijon University Hospital, the Regional Council of Burgundy, the project ANR (2010 FOETOCILPATH N° BLAN 1122 01 to T.A.B.). Finally, the authors would like to thank the NHLBI GO Exome Sequencing Project and its ongoing studies which produced and provided exome variant calls for comparison: the Lung GO Sequencing Project (HL-102923), the WHI Sequencing Project (HL-102924), the Broad GO Sequencing Project (HL-102925), the Seattle GO Sequencing Project (HL-102926) and the Heart GO Sequencing Project (HL-103010).

References

1. Baraitser M. The orofaciodigital (OFD) syndromes. J Med Genet. 1986; 23:116–9. [PubMed: 3712388]
2. Gurrieri F, Franco B, Toriello H, Neri G. Oral-facial-digital syndromes: review and diagnostic guidelines. Am J Med Genet A. 2007; 143A:3314–23. [PubMed: 17963220]

3. Giorgio G, Alfieri M, Prattichizzo C, Zullo A, Cairo S, Franco B. Functional characterization of the OFD1 protein reveals a nuclear localization and physical interaction with subunits of a chromatin remodeling complex. Mol Biol Cell. 2007; 18:4397–404. [PubMed: 17761535]
4. Valente EM, Logan CV, Mougou-Zerelli S, Lee JH, Silhavy JL, Brancati F, Iannicelli M, Travaglini L, Romani S, Illi B, Adams M, Szymanska K, Mazzotta A, Lee JE, Tolentino JC, Swistun D, Salpietro CD, Fede C, Gabriel S, Russ C, Cibulskis K, Sougnez C, Hildebrandt F, Otto EA, Held S, Diplas BH, Davis EE, Mikula M, Strom CM, Ben-Zeev B, Lev D, Sagie TL, Michelson M, Yaron Y, Krause A, Boltshauser E, Elkhartoufi N, Roume J, Shalev S, Munnich A, Saunier S, Inglehearn C, Saad A, Alkindy A, Thomas S, Vekemans M, Dallapiccola B, Katsanis N, Johnson CA, Attié-Bitach T, Gleeson JG. Mutations in TMEM216 perturb ciliogenesis and cause Joubert, Meckel and related syndromes. Nat Genet. 2010; 42:619–25. [PubMed: 20512146]
5. Adly N, Alhashem A, Ammari A, Alkuraya FS. Ciliary Genes TBC1D32/C6orf170 and SCLT1 are Mutated in Patients with OFD Type IX. Hum Mutat. 2014; 35:36–40. [PubMed: 24285566]
6. Thomas S, Legendre M, Saunier S, Bessières B, Alby C, Bonnière M, Toutain A, Loeuillet L, Szymanska K, Jossic F, Gaillard D, Yacoubi MT, Mougou-Zerelli S, David A, Barthez M-A, Ville Y, Bole-Feysot C, Nitschke P, Lyonnet S, Munnich A, Johnson CA, Encha-Razavi F, Cormier-Daire V, Thauvin-Robinet C, Vekemans M, Attié-Bitach T. TCTN3 mutations cause Mohr-Majewski syndrome. Am J Hum Genet. 2012; 91:372–8. [PubMed: 22883145]
7. Huang L, Szymanska K, Jensen VL, Janecke AR, Innes AM, Davis EE, Frosk P, Li C, Willer JR, Chodirker BN, Greenberg CR, McLeod DR, Bernier FP, Chudley AE, Müller T, Shboul M, Logan CV, Loucks CM, Beaulieu CL, Bowie RV, Bell SM, Adkins J, Zuniga FI, Ross KD, Wang J, Ban MR, Becker C, Nürnberg P, Douglas S, Craft CM, Akimenko M-A, Hegele RA, Ober C, Utermann G, Bolz HJ, Bulman DE, Katsanis N, Blacque OE, Doherty D, Parboosingh JS, Leroux MR, Johnson CA, Boycott KM. TMEM237 is mutated in individuals with a Joubert syndrome related disorder and expands the role of the TMEM family at the ciliary transition zone. Am J Hum Genet. 2011; 89:713–30. [PubMed: 22152675]
8. Lopez E, Thauvin-Robinet C, Reversade B, Khartoufi NE, Devisme L, Holder M, Ansart-Franquet H, Avila M, Lacombe D, Kleinfinger P, Kaori I, Takanashi J-I, Le Merrer M, Martinovic J, Noel C, Shboul M, Ho L, Guven Y, Razavi F, Burglen L, Gigot N, Darmency-Stamboul V, Thevenon J, Aral B, Kayserili H, Huet F, Lyonnet S, Le Caignec C, Franco B, Riviere J-B, Faivre L, Attie-Bitach T. C5orf42 is the major gene responsible for OFD syndrome type VI. Hum Genet. 2014; 133:367–77. [PubMed: 24178751]
9. Huber C, Cormier-Daire V. Ciliary disorder of the skeleton. Am J Med Genet C Semin Med Genet. 2012; 160C:165–74. [PubMed: 22791528]
10. Phadke SR, Pahi J, Pandey A, Agarwal SS. Oral-facial-digital syndrome with acromelic short stature: a new variant--overlap with Ellis Van Creveld syndrome. Clin Dysmorphol. 1999; 8:185–8. [PubMed: 10457851]
11. Li H, Durbin R. Fast and accurate short read alignment with Burrows-Wheeler transform. Bioinforma Oxf Engl. 2009; 25:1754–60.
12. McKenna A, Hanna M, Banks E, Sivachenko A, Cibulskis K, Kernytsky A, Garimella K, Altshuler D, Gabriel S, Daly M, DePristo MA. The Genome Analysis Toolkit: a MapReduce framework for analyzing next-generation DNA sequencing data. Genome Res. 2010; 20:1297–303. [PubMed: 20644199]
13. Pazour GJ, Baker SA, Deane JA, Cole DG, Dickert BL, Rosenbaum JL, Witman GB, Besharse JC. The intraflagellar transport protein, IFT88, is essential for vertebrate photoreceptor assembly and maintenance. J Cell Biol. 2002; 157:103–13. [PubMed: 11916979]
14. Gervais FG, Singaraja R, Xanthoudakis S, Gutekunst C-A, Leavitt BR, Metzler M, Hackam AS, Tam J, Vaillancourt JP, Houtzager V, Rasper DM, Roy S, Hayden MR, Nicholson DW. Recruitment and activation of caspase-8 by the Huntingtin-interacting protein Hip-1 and a novel partner Hippi. Nat Cell Biol. 2002; 4:95–105. [PubMed: 11788820]
15. Cole DG, Diener DR, Himelblau AL, Beech PL, Fuster JC, Rosenbaum JL. Chlamydomonas kinesin-II-dependent intraflagellar transport (IFT): IFT particles contain proteins required for ciliary assembly in Caenorhabditis elegans sensory neurons. J Cell Biol. 1998; 141:993–1008. [PubMed: 9585417]

16. Follit JA, Xu F, Keady BT, Pazour GJ. Characterization of mouse IFT complex B. Cell Motil Cytoskeleton. 2009; 66:457–68. [PubMed: 19253336]
17. Murcia NS, Richards WG, Yoder BK, Mucenski ML, Dunlap JR, Woychik RP. The Oak Ridge Polycystic Kidney (orpk) disease gene is required for left-right axis determination. Dev Camb Engl. 2000; 127:2347–55.
18. Houde C, Dickinson RJ, Houtzager VM, Cullum R, Montpetit R, Metzler M, Simpson EM, Roy S, Hayden MR, Hoodless PA, Nicholson DW. Hippi is essential for node cilia assembly and Sonic hedgehog signaling. Dev Biol. 2006; 300:523–33. [PubMed: 17027958]
19. Sun Z, Amsterdam A, Pazour GJ, Cole DG, Miller MS, Hopkins N. A genetic screen in zebrafish identifies cilia genes as a principal cause of cystic kidney. Dev Camb Engl. 2004; 131:4085–93.
20. Lunt SC, Haynes T, Perkins BD. Zebrafish ift57, ift88, and ift172 intraflagellar transport mutants disrupt cilia but do not affect hedgehog signaling. Dev Dyn Off Publ Am Assoc Anat. 2009; 238:1744–59.
21. Cavalcanti DP, Huber C, Sang K-HLQ, Baujat G, Collins F, Delezoide A-L, Dagoneau N, Le Merrer M, Martinovic J, Mello MFS, Vekemans M, Munnich A, Cormier-Daire V. Mutation in IFT80 in a fetus with the phenotype of Verma-Naumoff provides molecular evidence for Jeune-Verma-Naumoff dysplasia spectrum. J Med Genet. 2011; 48:88–92. [PubMed: 19648123]
22. McIntyre JC, Davis EE, Joiner A, Williams CL, Tsai I-C, Jenkins PM, McEwen DP, Zhang L, Escobado J, Thomas S, Szymanska K, Johnson CA, Beales PL, Green ED, Mullikin JC, Sabo A, Muzny DM, Gibbs RA, Attié-Bitach T, Yoder BK, Reed RR, Katsanis N, Martens JR. NISC Comparative Sequencing Program. Gene therapy rescues cilia defects and restores olfactory function in a mammalian ciliopathy model. Nat Med. 2012; 18:1423–8. [PubMed: 22941275]
23. Aldahmesh MA, Li Y, Alhashem A, Anazi S, Alkuraya H, Hashem M, Awaji AA, Sogaty S, Alkharashi A, Alzahrani S, Al Hazzaa SA, Xiong Y, Kong S, Sun Z, Alkuraya FS. IFT27, encoding a small GTPase component of IFT particles, is mutated in a consanguineous family with Bardet-Biedl syndrome. Hum Mol Genet. 2014; 23:3307–15. [PubMed: 24488770]
24. Beales PL, Bland E, Tobin JL, Bacchelli C, Tuysuz B, Hill J, Rix S, Pearson CG, Kai M, Hartley J, Johnson C, Irving M, Elcioglu N, Winey M, Tada M, Scambler PJ. IFT80, which encodes a conserved intraflagellar transport protein, is mutated in Jeune asphyxiating thoracic dystrophy. Nat Genet. 2007; 39:727–9. [PubMed: 17468754]
25. Arts HH, Bongers EMHF, Mans DA, van Beersum SEC, Oud MM, Bolat E, Spruijt L, Cornelissen EAM, Schuurs-Hoeijmakers JHM, de Leeuw N, Cormier-Daire V, Brunner HG, Knoers NVAM, Roepman R. C14ORF179 encoding IFT43 is mutated in Sensenbrenner syndrome. J Med Genet. 2011; 48:390–5. [PubMed: 21378380]
26. Perrault I, Saunier S, Hanein S, Filhol E, Bizet AA, Collins F, Salih MAM, Gerber S, Delphin N, Bigot K, Orssaud C, Silva E, Baudouin V, Oud MM, Shannon N, Le Merrer M, Roche O, Pietrement C, Goumid J, Baumann C, Bole-Feysot C, Nitschke P, Zahrate M, Beales P, Arts HH, Munnich A, Kaplan J, Antignac C, Cormier-Daire V, Rozet J-M. Mainzer-Saldino syndrome is a ciliopathy caused by IFT140 mutations. Am J Hum Genet. 2012; 90:864–70. [PubMed: 22503633]
27. Baujat G, Huber C, El Hokayem J, Caumes R, Do Ngoc Thanh C, David A, Delezoide A-L, Dieux-Coeslier A, Estournet B, Francannet C, Kayirangwa H, Lacaille F, Le Bourgeois M, Martinovic J, Salomon R, Sigaudy S, Malan V, Munnich A, Le Merrer M, Le Quan Sang KH, Cormier-Daire V. Asphyxiating thoracic dysplasia: clinical and molecular review of 39 families. J Med Genet. 2013; 50:91–8. [PubMed: 23339108]
28. Schmidts M, Arts HH, Bongers EMHF, Yap Z, Oud MM, Antony D, Duijkers L, Emes RD, Stalker J, Yntema J-BL, Plagnol V, Hoischen A, Gilissen C, Forsythe E, Lausch E, Veltman JA, Roeleveld N, Superti-Furga A, Kutkowska-Kazmierczak A, Kamsteeg E-J, Elçioğlu N, van Maarle MC, Graul-Neumann LM, Devriendt K, Smithson SF, Wellesley D, Verbeek NE, Hennekam RCM, Kayserili H, Scambler PJ, Beales PL, Knoers NV, Roepman R, Mitchison HM. UK10K. Exome sequencing identifies DYNC2H1 mutations as a common cause of asphyxiating thoracic dystrophy (Jeune syndrome) without major polydactyly, renal or retinal involvement. J Med Genet. 2013; 50:309–23. [PubMed: 23456818]
29. Schmidts M, Frank V, Eisenberger T, Al Turki S, Bizet AA, Antony D, Rix S, Decker C, Bachmann N, Bald M, Vinke T, Toenshoff B, Di Donato N, Neuhann T, Hartley JL, Maher ER, Bogdanović R, Peco-Antić A, Mache C, Hurles ME, Joksić I, Guć-Šćekić M, Dobricic J,

Brankovic-Magic M, Bolz HJ, Pazour GJ, Beales PL, Scambler PJ, Saunier S, Mitchison HM, Bergmann C. Combined NGS approaches identify mutations in the intraflagellar transport gene IFT140 in skeletal ciliopathies with early progressive kidney Disease. Hum Mutat. 2013; 34:714–24. [PubMed: 23418020]

30. Schneider RA, Hu D, Helms JA. From head to toe: conservation of molecular signals regulating limb and craniofacial morphogenesis. Cell Tissue Res. 1999; 296:103–9. [PubMed: 10199970]
31. Krock BL, Perkins BD. The intraflagellar transport protein IFT57 is required for cilia maintenance and regulates IFT-particle-kinesin-II dissociation in vertebrate photoreceptors. J Cell Sci. 2008; 121:1907–15. [PubMed: 18492793]

Figure 1. Clinical features of the subjects with unclassified OFDS

A) Family tree with the three affected cases; B and C) Pictures and X-Ray (respectively of subjects II-1 and II-2) showing the clinical hallmarks overlapping OFD (median pseudo cleft of upper lip, oral frenulae, pre- and post-polysyndactyly) and EVCS (missing incisors, short stature with mesomelic limb shortening). Skeleton features included additional brachymesophalangia, stocky femoral necks, and vertebral notches. Brain MRI was normal.

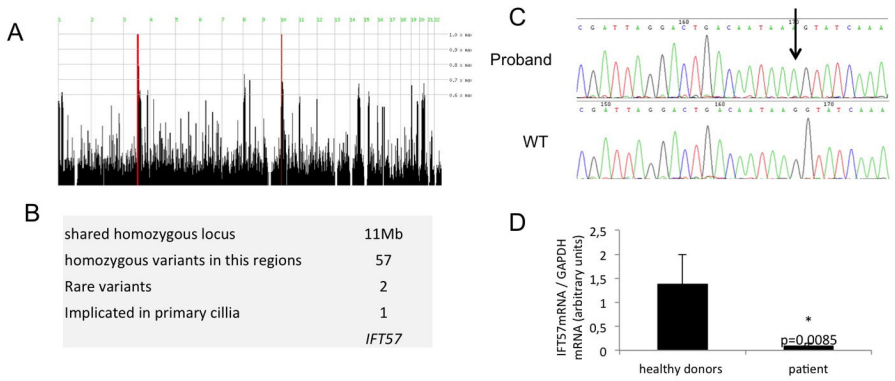

Figure 2. Evidence of the pathogenicity of the IFT57 homozygous p.Lys259Lys mutation

A) Homozygosity mapping in Subjects 2 and 3 identifying 2 shared homozygous runs on chromosome 3 and 10, totaling 11 megabases B) Whole exome sequencing for Subject 1, interpretation and variant prioritization focused on variants included in the homozygous regions. C) Sanger sequencing confirmed the familial segregation of the IFT57 variant in the three affected sibs. D) IFT57 cDNA was quantified in cultured fibroblasts, demonstrating a lower quantity of mRNA in the case than in multiple controls.

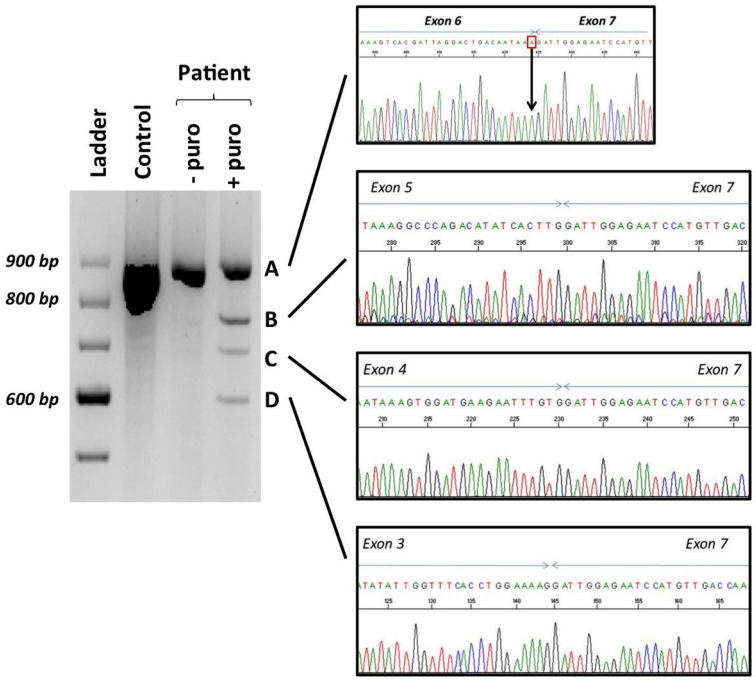

Figure 3. The synonymous c.777G>A substitution in exon 6 affects IFT57 pre-mRNA splicing

A) Exon 6 is present in the normal transcripts. The G>A substitution identified at the genomic level is detected in all IFT57 normal mRNAs. B) In frame exon 6 skipping. C) In frame skipping of exons 5 and 6. D) Out of frame skipping of exons 4, 5 and 6. Legend: − puro: no puromycin treatment, + puro: puromycine treatment

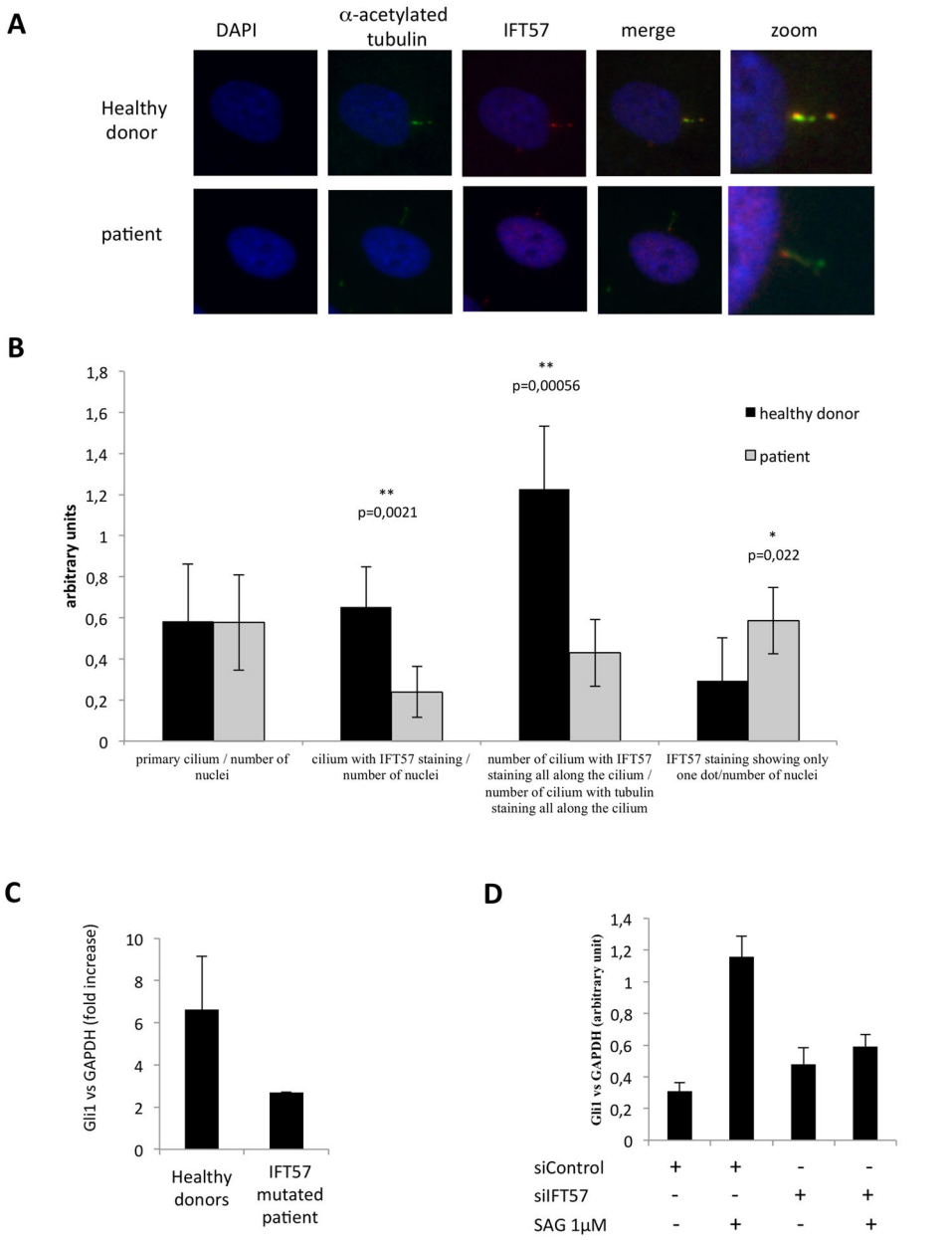

Figure 4. Functional impact of the mutation on ciliary transport

A) Immunofluorescence showing decreased anterograde ciliary transport in the subject's fibroblasts. IFT57 staining was low and restricted in most cells to the ciliary bases compared with control cells, which showed base and tip staining. B) Count of ciliary transport showing comparable ciliary number but decreased ciliary tip staining, black bar: healthy control; grey bar: subject C) Decreased GLI1 transcription activation secondary to lowered SHH signaling pathway in the subject's fibroblasts compared with healthy controls (representative experiment of 4) and in control fibroblasts after siRNA IFT57 delivery (representative experiment of 3).